lubricants

MDPI

Article

Tribocorrosion Response of Surface-Modified Ti in a 0.9% NaCl Solution

Richard Bailey

School of Engineering and Sustainable Development, Faculty of Technology, De Montfort University, Leicester LE1 9BH, UK; richard.bailey@dmu.ac.uk

Received: 13 August 2018; Accepted: 17 September 2018; Published: 25 September 2018

Abstract: Titanium use is limited due to its poor tribological properties, and thermal oxidation (TO) and pack carburisation with limited oxygen diffusion (PCOD) are just two of the surface treatments that can be used to enhance the surface properties of Ti. In this study, commercially pure titanium was surface modified using thermal oxidation (TO) and pack carburisation with limited oxygen diffusion (PCOD). Samples were tribological tested in a 0.9% NaCl solution under a contact load of 20 N to investigate the mechanical and electrochemical response of the surface treatments. The tests conducted show that a clear benefit can be obtained in terms of the overall material loss rate using both TO and PCOD. The TO and PCOD treatments generate very different surface structures: TO produces a rutile TiO_2 surface film and the PCOD treatment produces a TiC network structure. Both treatments improve the load bearing capacity with the assistance of an oxygen diffusion zone (ODZ). When subjected to sliding contact in a 0.9% NaCl solution, the results show the PCOD-Ti produced the best overall results, with a material loss rate 7.5 times lower than untreated Ti and 2.4 times lower than TO-Ti. The improved wear rate of the PCOD-Ti is attributed to the TiC network structure. The TO-Ti suffers from rapid film failure and high friction. The reduced material loss rate (MLR) of the TO-Ti is attributed to the hard wearing ODZ.

Keywords: titanium; thermal oxidation; carburisation; corrosion; wear; tribology; tribocorrosion

1. Introduction

Titanium and its alloys are a fundamental biomedical material, due to their high strength, low weight, and excellent corrosion resistance [1,2]. Within the biomedical sector, titanium is frequently used in orthopaedic, orthodontic, and cardiovascular applications [3,4]. However, almost all current applications are static and do not contain any contacting surfaces in relative motion. This is due to the well-documented tendency for titanium to seize when in sliding contact [5,6]. When titanium is used as an implant material, its poor tribological performance can result in high levels of wear particle accumulation in the surrounding tissue. This not only inhibits the service life of the implant, but can also cause severe allergic reactions to the implant user [7,8].

Over the years, various surface treatments have been developed to improve the plasticity index at the surface of titanium while maintaining its bulk characteristics. Thermochemical treatments have gained significant interest, with Boronising [9], carburising [10], nitriding [11], and oxidising [12] all being used to enhance the surface hardness of titanium. All the aforementioned treatments are able to decrease wear and improve upon the corrosion resistance of base titanium substrate. Of these thermochemical treatments, TO is low cost and shows promising results [13]. TO has been shown to greatly improve the corrosion resistance of titanium through the expansion of its native oxide film [14,15]. However, when subjected to sliding contact, the adhesion of the expanded titanium dioxide film limits the contact load before failure and thus the effectiveness [16–18].

Recently, a new pack carburisation technique has been developed and optimised, this treatment incorporates both oxygen and carbon into the titanium substructure. This process is known as PCOD and results in a multilayer structure [19]. The key characteristics of this treatment process are the formation of a carbon rich network-like structure at the titanium surface and an extended subsurface ODZ. This results in a surface hardness in the region of 2500 HV [20]. Initial electrochemical and tribo-electrochemical testing of PCOD-treated Ti suggests reduced wear, reduced friction, and a negligible impact on the corrosion performance over that of untreated Ti [21].

To date, PCOD-Ti has only ever been compared with TO-Ti and CP-Ti in unlubricated dry sliding conditions [20]. In the work presented, titanium was subjected to thermochemical conversion-treatment using both TO and PCOD. The resulting electrochemical and tribo-electrochemical performance of the treated Ti was evaluated in a 0.9% NaCl solution. The results were then correlated to the different surface and subsurface structures generated during treatment. This work demonstrates the effectiveness of the PCOD treatment at improving the tribocorrosion response of Ti, against a similarly low cost surface treatment.

2. Experimental

2.1. Sample Preparation and Characterisation

Commercially pure, grade 2 titanium (Ti) was used as the substrate material during this study. Before surface modification, the samples were cut from a 2 mm thick plate into square samples of a 20 mm length. To generate a constant surface, all samples were ground progressively with SiC to a grit of P1200, and this resulted in a surface roughness of 0.2 μm (Ra). Before surface treatments, the samples were cleaned in methanol with ultrasonic excitation for 15 min.

Thermal oxidation was undertaken by heating the Ti at 625 °C for 20 h in a standard muffle furnace (CWF, Carbolite Gero, Sheffield, UK). When thermally oxidising titanium, the rate of cooling has a substantial effect on the adhesion of the films generated [22], thus furnace cooling was implemented to improve film adhesion. This combination of temperature, duration, and cooling rate has been previously shown to produce a tightly adherent titanium dioxide (rutile) surface film [23]. Cross-sectional images of the resulting structure were taken using a Carl-Zeiss EvoHD 15 scanning electron microscope (SEM, Carl-Zeiss, Oberkochen, Germany) and can be observed in Figure 1a. The resulting structure shows that a film of ≈1 μm is generated. This is atop of an extended ODZ. The ODZ helps to increase the load bearing capacity though solid solution hardening [24], this effect is clearly demonstrated by the surface hardness measurements (taken using a Zwick/Roell ZHV MKII, Indentec, Brierley Hill, UK) recorded in Figure 2. When the surface hardness measurements of oxidised Ti are compared with those of untreated Ti, a clear increase in surface and subsurface hardness can be observed. X-Ray diffraction (XRD, Bruker, Billerica, MA, USA) analysis of the TO-Ti sample was undertaken using a Brucker D2 Phaser diffractometer using Cu K-α radiation (see Figure 3). The XRD analysis of TO-Ti samples shows clear peaks corresponding to the rutile form of TiO_2. Further investigation of the α-Ti peaks shows a clear shift compared to untreated Ti. This shift is associated with lattice expansion of the Ti HCP (Hexagonal close pack) structure from the dissolution of oxygen.

PCOD treatment was undertaken using the process detailed in Ref. [20]. The optimal conditions for the best tribological protection were found to occur when carburising was undertaken using a pack composition of six-part carbon, three-part $BaCO_3$, two-part $CaCO_3$, and one-part Na_2CO_3, and heated to 925 °C for 20 h. This combination has been proven to produce a subsurface feature referred to as a TiC network that shows uniformity to a depth of ≈7 μm. The SEM micrograph of the PCOD-Ti sample (Figure 1b) shows the TiC network structure produced during the treatment. Figure 1b also shows a pack residue that has formed on the surface of the samples. It is important to remove this before conducting any tests. This was removed through light polishing of the sample and then ultrasonic cleaning in methanol for 10 min. During the PCOD process, a substantial ODZ is

also generated and can have a substantial impact on the load bearing capacity of the treated sample. This is clearly shown in the surface hardness profiles displayed in Figure 2. The hardness profiles show the formation of an extremely high surface hardness of ≈2200 HV, which is comparable to that expected for TiC [25]. The difference in hardness of TO-TI and PCOD-Ti is more or less the same with increasing upload. This shows that the PCOD treatment not only produces a hard surface, but also a subsurface with an increased load bearing capacity, thanks to an extended ODZ. XRD analysis of the PCOD samples allows for the clear identification of TiC with very predominate peaks, suggesting a substantial coverage of TiC. It is also possible to identify the shifted α-Ti peaks associated with oxygen diffusion. Previous studies looking at the PCOD treatment used glow discharge optical spectroscopy (GDOS, Leco GDS850, LECO Corporation, St. Joseph, MI, USA) and energy dispersive spectroscopy (EDS, EvoHD 15, Carl-Zeiss, Oberkochen, Germany) to relate the network structure with a high carbon concentration [20]. Although TiC is identified in the XRD data, with the formation of TiC occurring through the reduction of TiO_x, mixed TiC_xO_x phases cannot be discounted.

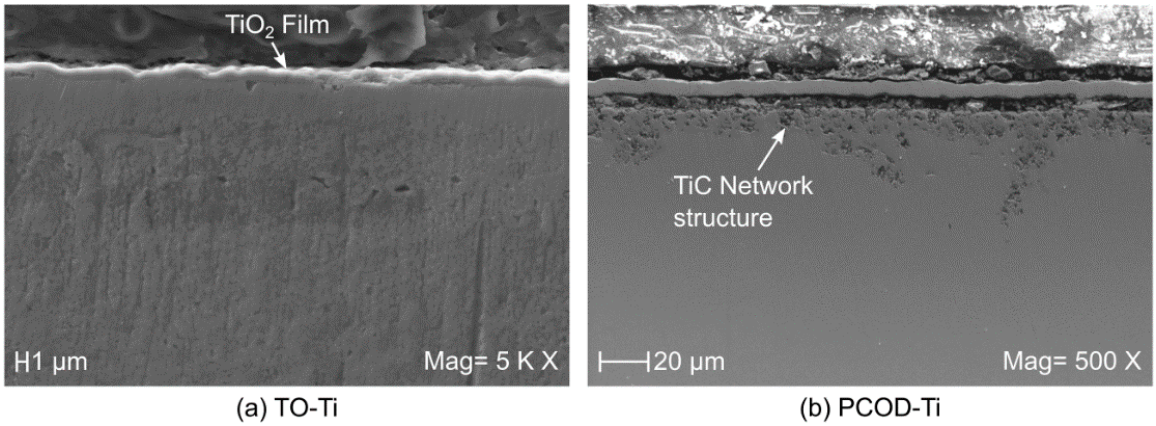

Figure 1. Cross-sectional SEM images showing the resulting surface and subsurface structures generated after: (**a**) TO and (**b**) PCOD.

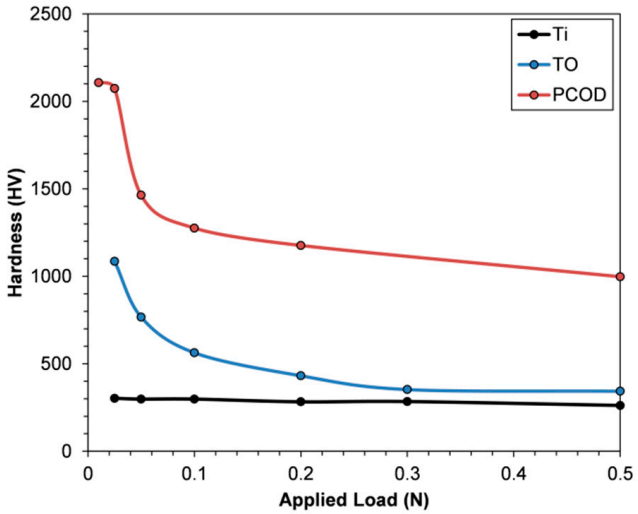

Figure 2. Surface hardness profiles produced by testing CP-Ti, TO-Ti, and PCOD-Ti.

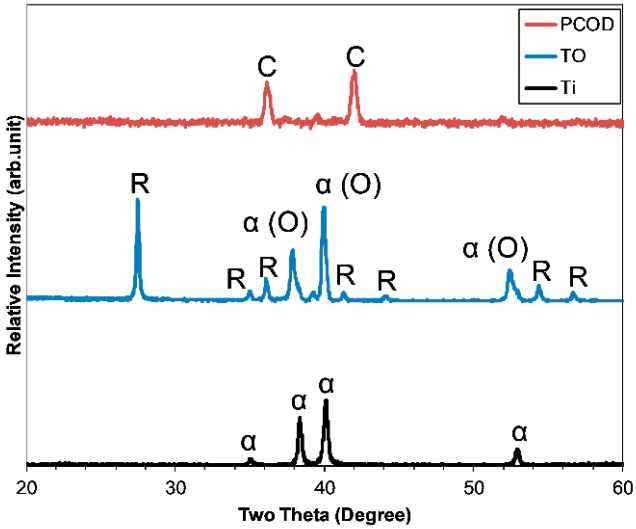

Figure 3. XRD patterns generated form CP-Ti, TO-Ti, and PCOD-Ti. Peak classifications are as follows: Alpha titanium (α), oxygen rich alpha titanium (α (O)), rutile titanium dioxide (R), and titanium carbide (C).

2.2. Corrosion Testing

When investigating biomedical metals, 0.9% NaCl (saline) solution is often used as an initial baseline test for understanding the fundamental response of the metal or coating [21,24]. This solution is effective as it is tribologically conservative (limited lubrication when compared with other biological mediums) and replicates human body salinity. During this study, both potentiodynamic and potentiostatic electrochemical corrosion tests were performed on the untreated and treated titanium samples. Tests were conducted using a traditional three-electrode cell utilising a saturated calomel reference electrode (SCE) and a platinum auxiliary electrode both connected to an ACM Gill AC potentiostat equipped with a data logger (Schematic can be found [23]). Once the working sample was loaded in the cell, the samples were cathodically charged to −500 mV for 180 s and this created a uniform starting point for all samples. All tests were conducted at room temperature (20 °C) and pressure.

Potentiodynamic measurements were recorded by sweeping from a cathodic to anodic of −400 mV/SCE to +1500 mV/SCE [vs. OCP (Open Circuit Potential)], using a sweep rate of 1 mVs^{-1}. Baseline OCP readings were recorded for 1 h prior to the potential sweep.

Current transient measurements were performed by holding the samples at a potential of 500 mV/SCE for 3600 s, with the current density recorded for the duration of the test.

2.3. Tribocorrosion Testing

Combined wear and corrosion tests were undertaken using a Teer Coting pin on disk tribometer, incorporating an electrochemical cell, a detained schematic of the setup can be found in [18]. To ensure comparable results, the exposed surface area of the sample was controlled. Lacquer was used to expose a surface area of 1.23 mm^2 to the electrolyte. During the tribocorrosion tests, a surface contact load of 20 N was applied to the sample with an 8 mm diameter alumina (Al_2O_3) ball manufactured by Trafalgar bearings. This contact combination results in a max Hertzian contact pressure at the surface of ≈1291 MPa and a max shear stress of ≈391 MPa at a depth of ≈42 µm from the surface. Using alumina removes any possible interaction with the counterface and the electrolyte, due to its inert nature. The tribometer was set to rotate at a speed of 60 rpm with a wear track diameter of 9 mm.

0.9% NaCl was again chosen as the test medium and was conducted at room temperature and pressure. During tribocorrosion testing, the OCP of the system and friction coefficient data were captured. Prior to testing, the samples were exposed to the electrolyte and allowed to stabilise for

30 min prior to surface contact. After stabilisation, the contact was initiated and lasted for 2 h. After the 2 h, the contact was removed and the materials' re-stabilisation was recorded for 30 min.

After tribocorrosion testing, the wear track of the samples was evaluated using a stylus profilometer (Mitutoyo SJ-400). Using eight sections of the wear track, the average area was calculated and the total wear track volume was then estimated. The total material loss rate (TMLR) was then evaluated using the volume (V), sliding distance (d_s), and applied load (L) by employing the following: TMLR = V/d_sL.

During tribocorrosion testing, it is possible to estimate the amount of material loss associated with the electrochemical interactions. Using the potentials generated during OCP testing, the Butler–Volmer equation can be used to calculate the anodic current passing through the wear track (i_a), as shown in Equation (1).

$$\log i_a = \frac{E_{corr} - E_c + a_c}{b_c} - \log\left(\frac{A_a}{A_c}\right) \quad (1)$$

The Butler–Volmer equation also uses the potential measured during sliding (E_c), the corrosion potential (E_{corr}), and the Tafel constants (a_c, b_c) extracted from the potential dynamic sweeps. The ratio between the wear track area (A_a) and the cathode area (A_c) is also needed. Once the current has been calculated, Faraday's law can be used to determine the approximate volume lost due to the electrochemical interactions [26–28].

3. Results and Discussion

3.1. Corrosion Testing

3.1.1. Potentiodynamic

The polarisation curves displayed in Figure 4 show that distinct characteristics are present for the different surface treatments presented. The untreated Ti shows the standard curve expected with a free corrosion potential value of ≈−300 mV/SCE and a consistent passive region present throughout the anodic potentials. The TO-Ti sample shows a large shift in the free corrosion potential to ≈+100 mV/SCE and a consistent passive region displaying an extremely low current density. This positive shift in OCP is as expected for TO-Ti and has been seen many time before [27,29,30], and has been attributed to the dense and tightly adherent TiO_2 rutile film acting as a barrier for the subsurface titanium. When evaluating the polarisation curve produced by the PCOD-Ti, there are two distinct differences observed from that of the CP-Ti. The first key difference is the observed positive shift in the corrosion potential and the second is an increase in the current density recorded during the anodic sweep. This behaviour has been previously reported for TiC films [31]. Unlike the Rutile TiO_2 film generated during thermal oxidation, the TiC spontaneously reacts with water, forming a TiO_2 surface film [32]. The conversion of TiC to TiO_2 can be attributed to the higher current densities observed during testing.

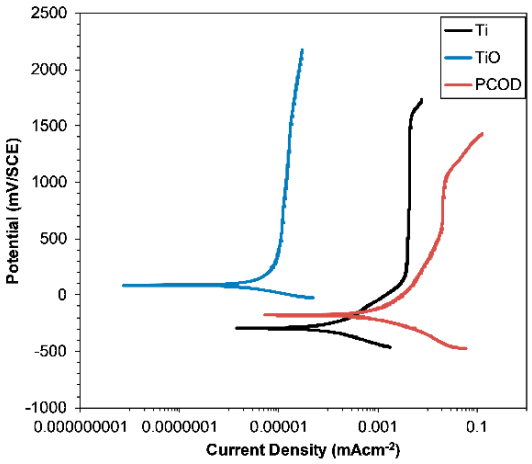

Figure 4. Polarisation curves recorded for CP-Ti, PCOD-Ti, and TO-Ti. All tests were conducted in a 0.9% NaCl medium with a sweep rate of 1 mVs^{-1}.

3.1.2. Potentiostatic

Potentiostatic testing was undertaken with the results displayed in Figure 5. Using Figure 4, we observe that 500 mV/SCE is within the passive region for all samples. The current transient responses of the untreated and treated Ti are presented using a log scale in both the abscissa and ordinate axis. When investigating transient current behaviour, it is important to consider both the point defect model and the high field theory to understand how ion flux changes at a material's surface [33,34]. When untreated Ti is exposed to an anodic current, the naturally occurring oxide film will expand by the mechanism described in Equation (2).

$$Ti^{+} + 2H_2O \rightarrow TiO_2 + 2H_2 \quad (2)$$

As the TiO_2 film thickens, the ion flux will reduce, thus leading to a lower conduction and current density (I). This change in current response over time (t) is described by Equation (3) [33,35], where A is the intercept and k is the gradient.

$$\log(I) = A - k\log(t) \quad (3)$$

When evaluating the film generated, the gradient gives a strong indication as to the thickness and porosity of the surface film. When $k = 1$, this characterises a thick, dense film; thinner films or more porous films would produce a gradient (k) < 1.

The data displayed in Figure 5 show the varying surface states of the treated Ti. When conducting transient testing, there is often an initial stage with lower curve gradients ($k \approx 0.5$) that is attributed to the small film thickness during the early stages of polarization. This has been reported by numerous authors in relation to Ti [33,35] and can be seen in both the Untreated and PCOD-Ti. As the polarisation time increases, the passive films thicken and the gradients of the lines increase and converge towards a k value of 1. This is particularly true for the untreated Ti that reaches $k = 1$ after ≈1000 s, which indicates the formation of a dense and tightly adherent film. The PCOD-Ti shows conformity to Equation (3), but does not generate the ideal value for k, with a gradient (k) of 0.75 in just 300 s, and this phenomenon has been previously observed [21].

The TO-Ti sample has extremely low current densities throughout the test; this is due to the barrier nature of the oxide film produced. The current transient behaviour does not follow that described by Equation (3), due to the thick oxide layer (≈1 µm) protecting the subsurface metal from the electrolyte. From both the current transient and potentiodynamic sweeps, there is a clear benefit from TO. Under static (non-tribological) corrosion testing in a 0.9% NaCl solution, the rutile film offers excellent corrosion protection.

The current transient data displayed in Figure 5 shows that the PCOD-Ti and untreated Ti are quite similar in their response, with both sets of data conforming to Equation (3). However, there are some significant differences, with one of them being related to the gradient of the PCOD-Ti (k = 0.75), which is much less than that measured for the untreated Ti (k = 1). When Ti is anodically charged it will encourage Equation (2). The increased thickness will improve the barrier nature of the oxide film, as demonstrated by the decreasing current density with time. The PCOD-Ti is shown to have a network-like structure that is predominately TiC. Interestingly, when TiC is exposed to a neutral solution, a TiO_2 boundary layer will be formed through hydrolysis [32] (see Equation (4)).

$$TiC + XH_2O \rightarrow TiO_2 \cdot H_2O + CH_4 \quad (4)$$

Avgustink et al., found that this film will be produced at the boundary interface and will form a thickness ranging from 100 to 150 Å. During the formation of the TiC network, the presence of mixed phases of Ti, C, and O cannot be discounted. This will result in differing surface kinetics, depending on composition, and will result in an increased defect density. With a surface containing multiple phases, galvanic cells can develop and result in faster dissociation [36]. The incorporation of C within TiO_2 will result in extra intersectional sites, allowing for greater ion transportation.

Another noticeable difference between the PCOD-Ti and the untreated Ti is the speed at which each sample reaches linearity. The PCOD-Ti reaches linearity in around 100 s compared with Ti, which takes 1000 s. This conforms to the premise that a TiO_2 film is rapidly generated on the surface of the PCOD-Ti when in contact with water. However, this film is less dense and has a greater porosity than the TiO_2 generated at the surface of untreated titanium.

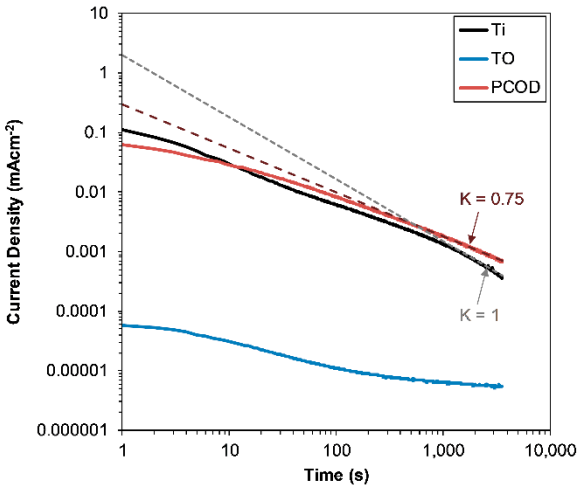

Figure 5. Current transient response of untreated Ti, TO-Ti, and PCOD-TI in the log(I) vs. log(t) scale. All tests conducted in a 0.9% NaCl solution at an anodic potential of +500 mV for a duration of 3600 s.

3.2. OCP Tribocorrosion Testing

During tribocorrosion testing, both the friction coefficient and surface potential were recorded, and the results from these tests can be observed in Figure 6. From the data collected during sliding contact, the untreated Ti exhibited a constant friction coefficient of ≈0.5 throughout the 2 h test. The OCP data collected for the untreated Ti shows a clear activation of the surface when sliding is initiated, and a sudden drop in potential from −200 mV/SCE to 1080 mV/SCE is observed. This reaction is typical for untreated Ti, and the large drop in OCP is associated with the activation of Ti via the abrasive removal of the oxide film. Exposure of the subsurface Ti encourages the passivation of the exposed material within the wear track. The high and unstable friction coefficient is also typical for Ti and directly relates to the high levels of adhesive wear present within the wear track (see Figure 7a).

The wear track image for the untreated sample also reveals deep grooves within the breadth of the wear track with substantial amounts of cracking and delamination.

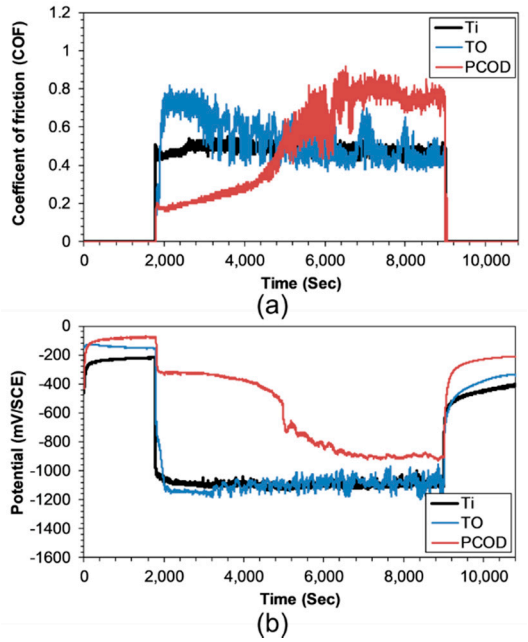

Figure 6. Coefficient of friction (**a**) and OCP (**b**) measurements made before, during, and after the application of a 20 N load in a 0.9% NaCl solution.

The TO-Ti has some significant differences compared to the untreated Ti in both the friction and OCP traces presented in Figure 6a,b, respectively. When looking into the OCP data, we observe an initial stabilisation period when there is no sliding contact, and the OCP reading for the TO-Ti is highest of all the samples tested, including the PCOD-Ti. This result backs up the data generated during potentiostatic (Figure 5) and potentiodynamic (Figure 4) corrosion testing and suggests that the TiO_2 film generated during TO produces the least active surface. However, when subjected to sliding contact, we see a similar response to that observed in the untreated Ti sample and this is characterised by high unstable friction and a large drop in the OCP measurement. There are some subtle differences that should not be discounted and need to be discussed. During the onset of sliding, there is an initial stage when the friction and OCP deviate from those recorded in the untreated Ti. There is more of a gradual change in both friction and OCP, and is not observed in the untreated Ti. This change in the initial response is attributed to the TiO_2 surface film. However, under such an extreme load (20 N), the surface film is rapidly removed from the wear track. When investigating the wear track image displayed in Figure 7b, there is a clearly defined shear edge along the circumference of the wear track. Upon the application of surface contact, the TiO_2 surface film is rapidly removed from the surface due to a lack of sufficient adhesion with the subsurface ODZ. This is a well-documented issue associated with TO-Ti and is caused by a thermal mismatch between the oxide film and the subsurface Ti during cooling, this generates interfacial cracks. Prolonged cooling has been shown to be an effective method for reducing this scaling issue [22], as such furnace cooling was employed in this study. Although prolonged cooling can be effective at reducing the scaling issue, at a load of 20 N, it is still ineffectual at maintaining film integrity/adhesion. Another important feature noted from the data in Figure 6, is the period of increased friction from around 2000 s to 3100 s. The COF (0.7) is above the level observed for the untreated Ti and occurs while there is contact between the Al_2O_3 ball and the ODZ. This period of increased friction also coincides with a period of increased electrochemical activity, as indicated by the OCP measurements (Figure 6b). As the ODZ is removed from the wear track, both the friction COF and OCP data return to a level similar to that of untreated Ti, and this overall behavior has been

previously observed for TO-Ti [23]. The wear track morphology produced after the test (Figure 7b) shows characteristics that are very similar to untreated Ti, across the central breadth of the wear track.

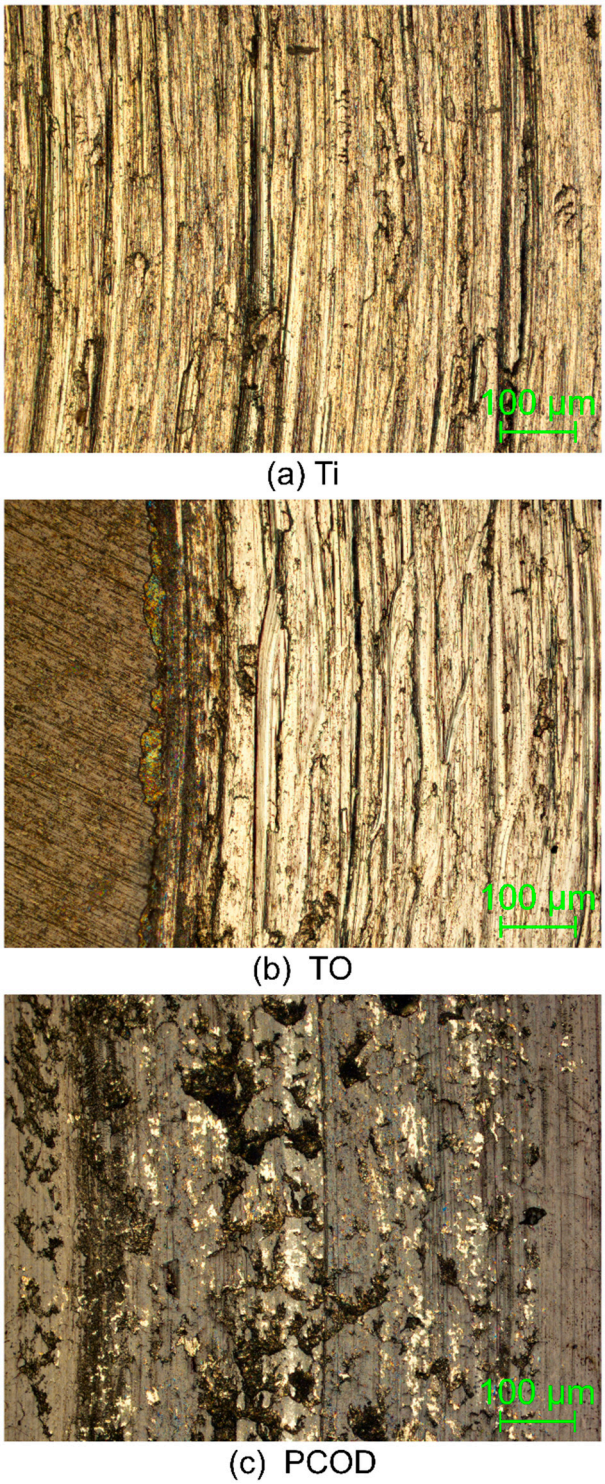

Figure 7. Optical microscope images (200× mag) showing the different wear mechanisms encountered by: CP-Ti (**a**), TO-Ti (**b**), and PCOD-Ti (**c**).

The data recorded for the PCOD-Ti shows a significantly different tribological and electrochemical response than that observed for the untreated and TO-Ti. The friction data displayed in Figure 6a shows three clear and distinct stages of the friction characteristics. There is an initial period from the

onset of sliding until 4400 s, when the COF gradually rises from 0.2 to 0.3, and this period also coincides with a gradual drop in potential (Figure 6b). After this initial period, there is then an accelerated increase in COF from around 0.3 to approximately 0.8. This also coincides with a significant drop in OCP. The initial low COF recorded is significantly lower than anything recorded for both the untreated and TO-Ti. This low COF can be attributed to the surface structures generated during the PCOD treatment. Unlike the TiO_2 film generated during TO, the network-like structure has no obvious interfacial boundary in which film failure can occur, thus resulting in excellent adhesion. The PCOD treatment also benefits from the increased subsurface hardness, thanks to the extended ODZ (Figure 2). The load bearing capacity and the excellent adhesion of the TiC network allow for limited protection of the sample when subjected to a 20 N load. During the initial stages of the test, hydrolysis of the TiC will produce a TiO_2 film within the wear track. Removal and subsequent rebuilding of this TiO_2 film are responsible for the OCP measurements recorded during the initial phase of the test. Given the formation mechanism of the TiO_2 within the wear track interface, the oxide films generated are anticipated to be non-stoichiometric (TiO_{2n-1}). These oxygen deficient titanium oxides are often referred to as Magneli phases [37]. Magneli phases have been shown to exhibit reduced friction compared with pure Rutile TiO_2 and have been shown to develop on TiC coatings [32]. The presence of Magneli phases could be attributed to the reduced COF observed in the early stages of testing.

Once a sufficient level of wear has occurred, exposure of subsurface ODZ is inevitable and is associated with the gradual increase in both COF and OCP observed in Figure 6. As the ratio of ODZ to TiC network increases, both the COF and OCP measurements begin to conform to those recorded for the ODZ from the TO-Ti. The wear track morphology for the PCOD-Ti (Figure 7c) reveals exposure of the subsurface material. There are also large areas of oxide formation within the wear track, which has a smooth finish from progressive polishing. This is associated with the TiC network and remains present wherever there is a sufficient level of TiC cover, as highlighted in Figure 8. The ball crater image clearly shows that film formation is directly linked to the coverage of the TiC network. Where there is no network coverage, the wear track film is no longer observable and exposure of the ODZ is observed.

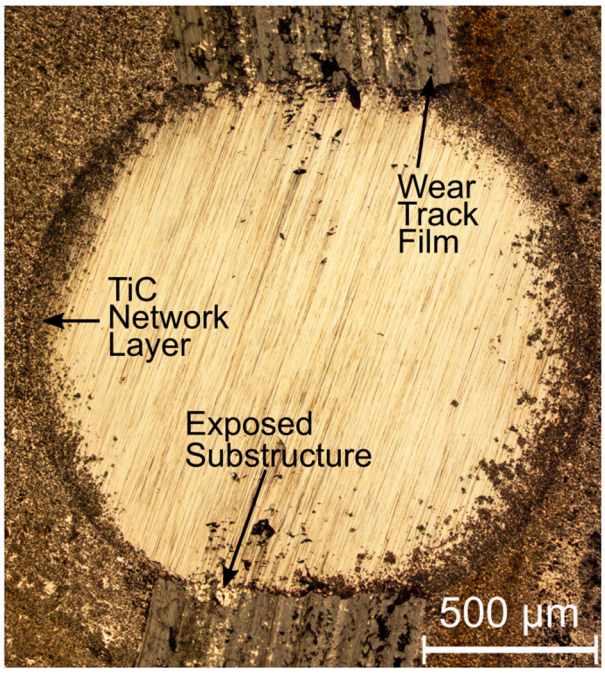

Figure 8. Ball Crater generated on the wear track produced by sliding in OCP conditions on the PCOD titanium, showing the wear depth relative to the network structure.

Wear Rates

The total material loss rate can be observed for all samples in Figure 9. The data presented shows a clear trend depending on the surface treatment used. The untreated Ti was less resistant to material loss. Both surface treatments used in this study demonstrate enhanced wear resistance, with the PCOD treatment reducing total wear by a factor of 7.6. When looking at the wear mechanism, the material loss is dominated by the mechanical interaction, rather than electrochemical processes. However, there are variations in the amount of chemical wear depending on the surface treatment. The PCOD sample shows significantly less chemical wear than both the thermally oxidised and untreated titanium. This reduced chemical wear can be attributed to the excellent adhesion and integrity of the TiC network, limiting subsurface exposure when subjected to high contact loads.

Another interesting phenomenon is the reduced wear rate measured from the TO samples. The friction traces and wear track images show that the total removal of the TiO_2 film from within the wear track happens almost instantaneously with the application of the load. Removal of the TiO_2 film resulted in high friction (≈0.7) during contact with the ODZ and then stabilisation to a value similar to that of the untreated Ti (≈0.5). This high unstable friction seems to have had little bearing on the overall wear rate. The ODZ generated during the TO process generates a region below the surface film that has improved wear resistance but offers none of the lower friction associated with rutile TiO_2. Wearing of the ODZ can also be attributed to the proportionally higher chemical wear measured. A previous study has shown that the ODZ demonstrates accelerated passivation, thus increasing the rate of wear track oxide produced after successive sliding contacts [23].

When considering the combined tribo-electrochemical performance of all three samples, the PCOD sample exhibits a superior wear resistance and load bearing capacity when exposed to the 0.9% NaCl solution. While the TiC network is present, the PCOD-Ti is able to provide low friction and increased wear resistance under combined wear and corrosion conditions.

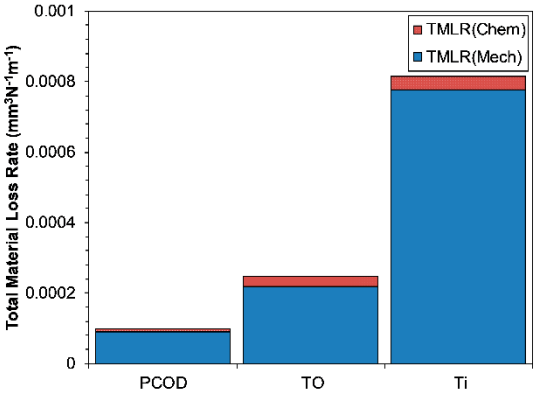

Figure 9. Specific total material loss rate for the untreated titanium, TO-Ti, and PCOD-Ti. Both the mechanical and chemical contributions to the loss rate are displayed.

4. Conclusions

1. Under static corrosive conditions, TO-Ti offers the best improvement in corrosive resistance, due to the thick, non-porous rutile surface film.
2. Both treated samples show significant material loss reductions when compared with untreated Ti. When compared with untreated Ti, the TO-Ti reduced material loss by 3.2 times and the PCOD-Ti reduced wear by 7.6 times.
3. Under tribo-electrochemical conditions, the PCOD treatment outperformed the TO treatment and was able to maintain limited protection when subjected to a contact load of 20 N. Low friction coefficients observed can be attributed to an oxygen deficient film formed during sliding contact.
4. The TiC network structure formed during the PCOD process shows excellent adhesion and an ability to sustain high loads without critical failure.

Funding: This research received no external funding.

Acknowledgments: I would like to thank De Montfort University for the financial support provided. I would also like to acknowledge Y. Sun for his involvement in the initial studies and development of the PCOD treatment.

Conflicts of Interest: The author declares no conflict of interest.

References

1. Gao, A.; Hang, R.; Bai, L.; Tang, B.; Chu, P.K. Electrochemical surface engineering of titanium-based alloys for biomedical application. *Electrochim. Acta* **2018**, *271*, 699–718. [CrossRef]
2. Mohammed, M.T. Development of a new metastable beta titanium alloy for biomedical applications. *Karbala Int. J. Mod. Sci.* **2017**, *3*, 224–230. [CrossRef]
3. Xiao, M.; Chen, Y.M.; Biao, M.N.; Zhang, X.D.; Yang, B.C. Bio-functionalization of biomedical metals. *Mater. Sci. Eng. C* **2017**, *70*, 1057–1070. [CrossRef] [PubMed]
4. Asri, R.I.M.; Harun, W.S.W.; Samykano, M.; Lah, N.A.C.; Ghani, S.A.C.; Tarlochan, F.; Raza, M.R. Corrosion and surface modification on biocompatible metals: A review. *Mater. Sci. Eng. C* **2017**, *77*, 1261–1274. [CrossRef] [PubMed]
5. Dong, H.; Bell, T. Enhanced wear resistance of titanium surfaces by a new thermal oxidation treatment. *Wear* **2000**, *238*, 131–137. [CrossRef]
6. Bloyce, A. Surface engineering of titanium alloys for wear protection. *Proc. Inst. Mech. Eng.* **1998**, *212*, 467–476. [CrossRef]
7. Ehtemam-Haghighi, S.; Prashanth, K.G.; Attar, H.; Chaubey, A.K.; Cao, G.H.; Zhang, L.C. Evaluation of mechanical and wear properties of TixNb7Fe alloys designed for biomedical applications. *Mater. Des.* **2016**, *111*, 592–599. [CrossRef]
8. Haghighi, S.E.; Lu, H.B.; Jian, G.Y.; Cao, G.H.; Habibi, D.; Zhang, L.C. Effect of α martensite on the microstructure and mechanical properties of beta-type Ti–Fe–Ta alloys. *Mater. Des.* **2015**, *76*, 47–54. [CrossRef]
9. Sivakumar, B.; Pathak, L.C.; Singh, R. Fretting corrosion response of boride coated titanium in ringer's solution for bio-implant use: Elucidation of degradation mechanism. *Tribol. Int.* **2018**, *127*, 219–230. [CrossRef]
10. Brama, M.; Rhodes, N.; Hunt, J.; Ricci, A.; Teghil, R.; Migliaccio, S.; Rocca, C.D.; Leccisotti, S.; Lioi, A.; Scandurra, M.; et al. Effect of titanium carbide coating on the osseointegration response in vitro and in vivo. *Biomaterials* **2007**, *28*, 595–608. [CrossRef] [PubMed]
11. Wang, X.; Bai, S.; Li, F.; Li, D.; Zhang, J.; Tian, M.; Zhang, Q.; Tong, Y.; Zhang, Z.; Wang, G.; et al. Effect of plasma nitriding and titanium nitride coating on the corrosion resistance of titanium. *J. Prosthet. Dent.* **2016**, *116*, 450–456. [CrossRef] [PubMed]
12. Aniołek, K. The influence of thermal oxidation parameters on the growth of oxide layers on titanium. *Vacuum* **2017**, *144*, 94–100. [CrossRef]
13. Dong, H.; Bell, T. Designer surfaces for titanium components. *Anti-Corros. Methods. Mater.* **1999**, *46*, 338–346. [CrossRef]
14. Güleryüz, H.; Çimenoğlu, H. Effect of thermal oxidation on corrosion and corrosion-wear behaviour of a Ti–6Al–4V alloy. *Biomaterials* **2004**, *25*, 3325–3333. [CrossRef] [PubMed]
15. Kumar, S.; Sankara Narayanan, T.S.N.; Ganesh Sundara Raman, S.; Seshadri, S.K. Fretting corrosion behaviour of thermally oxidized CP-ti in ringer's solution. *Corros. Sci.* **2010**, *52*, 711–721. [CrossRef]
16. Aniołek, K.; Kupka, M.; Barylski, A. Sliding wear resistance of oxide layers formed on a titanium surface during thermal oxidation. *Wear* **2016**, *356–357*, 23–29. [CrossRef]
17. Alansari, A.; Sun, Y. A comparative study of the mechanical behaviour of thermally oxidised commercially pure titanium and zirconium. *J. Mech. Behav. Biomed. Mater.* **2017**, *74*, 221–231. [CrossRef] [PubMed]
18. Dearnley, P.A.; Dahm, K.L.; Çimenoğlu, H. The corrosion-wear behaviour of thermally oxidised CP-ti and Ti–6Al–4V. *Wear* **2004**, *256*, 469–479. [CrossRef]
19. Bailey, R.; Sun, Y. Pack carburisation of commercially pure titanium with limited oxygen diffusion for improved tribological properties. *Surf. Coat. Technol.* **2015**, *261*, 28–34. [CrossRef]
20. Bailey, R.; Sun, Y. An investigation into the effects of process conditions on the tribological performance of pack carburized titanium with limited oxygen diffusion. *J. Mater. Eng. Perform.* **2018**, *26*, 1–11. [CrossRef]
21. Bailey, R.; Sun, Y. Corrosion and tribocorrosion performance of pack-carburized commercially pure titanium with limited oxygen diffusion in a 0.9% NaCl solution. *J. Bio-Tribo-Corros.* **2018**, *4*, 6. [CrossRef]

22. Siva Rama Krishna, D.; Brama, Y.L.; Sun, Y. Thick rutile layer on titanium for tribological applications. *Tribol. Int.* **2007**, *40*, 329–334. [CrossRef]
23. Bailey, R.; Sun, Y. Corrosion and tribocorrosion performance of thermally oxidized commercially pure titanium in a 0.9% NaCl solution. *J. Mater. Eng. Perform.* **2015**, *24*, 1669–1678. [CrossRef]
24. Dong, H.; Li, X.Y. Oxygen boost diffusion for the deep-case hardening of titanium alloys. *Mater. Sci. Eng. A* **2000**, *280*, 303–310. [CrossRef]
25. Luo, Y.; Jiang, H.; Cheng, G.; Liu, H. Effect of carburization on the mechanical properties of biomedical grade titanium alloys. *J. Bionic Eng.* **2011**, *8*, 86–89. [CrossRef]
26. Landolt, D.; Mischler, S.; Stemp, M. Electrochemical methods in tribocorrosion: A critical appraisal. *Electrochim. Acta* **2001**, *46*, 3913–3929. [CrossRef]
27. Sun, Y.; Haruman, E. Effect of electrochemical potential on tribocorrosion behavior of low temperature plasma carburized 316L stainless steel in 1 M H_2SO_4 solution. *Surf. Coat. Technol.* **2011**, *205*, 4280–4290. [CrossRef]
28. Sun, Y.; Rana, V. Tribocorrosion behaviour of AISI 304 stainless steel in 0.5 M NaCl solution. *Mater. Chem. Phys.* **2011**, *129*, 138–147. [CrossRef]
29. Ashrafizadeh, A.; Ashrafizadeh, F. Structural features and corrosion analysis of thermally oxidized titanium. *J. Alloys Compd.* **2009**, *480*, 849–852. [CrossRef]
30. Kumar, S.; Sankara Narayanan, T.S.N.; Ganesh Sundara Raman, S.; Seshadri, S.K. Thermal oxidation of CP Ti—An electrochemical and structural characterization. *Mater. Charact.* **2010**, *61*, 589–597. [CrossRef]
31. Oláh, N.; Fogarassy, Z.; Furkó, M.; Balázsi, C.; Balázsi, K. Sputtered nanocrystalline ceramic TiC/amorphous C thin films as potential materials for medical applications. *Ceram. Int.* **2015**, *41*, 5863–5871. [CrossRef]
32. Avgustinik, A.I.; Drozdetskaya, G.V.; Ordan'yan, S.S. Reaction of titanium carbide with water. *Soviet Powder Metall. Met. Ceram.* **1967**, *6*, 470–473.
33. Raja, K.S.; Jones, D.A. Effects of dissolved oxygen on passive behavior of stainless alloys. *Corros. Sci.* **2006**, *48*, 1623–1638. [CrossRef]
34. Zhang, Y.; Macdonald, D.D.; Urquidi-Macdonald, M.; Engelhardt, G.R.; Dooley, R.B. Passivity breakdown on AISI type 403 stainless steel in chloride-containing borate buffer solution. *Corros. Sci.* **2006**, *48*, 3812–3823. [CrossRef]
35. Sun, Y. Depth-profiling electrochemical measurements of low temperature plasma carburised 316L stainless steel in 1 M H_2SO_4 solution. *Surf. Coat. Technol.* **2010**, *204*, 2789–2796. [CrossRef]
36. Schneider, M.; Kremmer, K.; Lämmel, C.; Sempf, K.; Herrmann, M. Galvanic corrosion of metal/ceramic coupling. *Corros. Sci.* **2014**, *80*, 191–196. [CrossRef]
37. Gardos, M.N.; Hong, H.; Winer, W.O. The effect of anion vacancies on the tribological properties of rutile (TiO_{2-x}), part II: Experimental evidence. *Tribol. Trans.* **1990**, *33*, 209–220. [CrossRef]

© 2018 by the author. Licensee MDPI, Basel, Switzerland. This article is an open access article distributed under the terms and conditions of the Creative Commons Attribution (CC BY) license (http://creativecommons.org/licenses/by/4.0/).